*Journal of Biomolecular NMR* **27:** 193–203, 2003.



# $^1H_C$ and $^1H_N$ total NOE correlations in a single 3D NMR experiment. $^{15}N$ and $^{13}C$ time-sharing in $t_1$ and $t_2$ dimensions for simultaneous data acquisition

Youlin Xia[a,b], Adelinda Yee[b,c], Cheryl H. Arrowsmith[b,c] & Xiaolian Gao[a,*]
[a]*Department of Chemistry, University of Houston, Houston, TX 77004-5003, U.S.A.;* [b]*Ontario Cancer Institute and Department of Medical Biophysics, The University of Toronto, Toronto, ON, Canada M5G 2M9;* [c]*Northeast Structural Genomics Consortium*

Received 14 January 2003; Accepted 13 May 2003

*Key words:* HSQC, NOESY, protein NMR, proteomics, simultaneous data acquisition, time-sharing

**Abstract**

Simultaneous data acquisition in time-sharing (TS) multi-dimensional NMR experiments has been shown an effective means to reduce experimental time, and thus to accelerate structure determination of proteins. This has been accomplished by spin evolution time-sharing of the X and Y heteronuclei, such as $^{15}N$ and $^{13}C$, in one of the time dimensions. In this work, we report a new 3D TS experiment, which allows simultaneous $^{13}C$ and $^{15}N$ spin labeling coherence in both $t_1$ and $t_2$ dimensions to give four NOESY spectra in a single 3D experiment. These spectra represent total NOE correlations between $^1H_N$ and $^1H_C$ resonances. This strategy of double time-sharing (2TS) results in an overall four-fold reduction in experimental time compared with its conventional counterpart. This 3D 2TS CN-CN-H HSQC-NOESY-HSQC pulse sequence also demonstrates improvements in water suppression, $^{15}N$ spectral resolution and sensitivity, which were developed based on 2D TS CN-H HSQC and 3D TS H-CN-H NOESY-HSQC experiments. Combining the 3D TS and the 3D 2TS NOESY experiments, NOE assignment ambiguities and errors are considerably reduced. These results will be useful for rapid protein structure determination to complement the effort of discerning the functions of diverse genomic proteins.

## Introduction

NMR-derived protein structures are based on interproton distance restraints obtained from $^{15}N$- and $^{13}C$-edited 2D, 3D and 4D NOESY data sets, torsion-angle restraints generated from various heteronuclear and homonuclear scalar coupling correlation experiments (Wagner, 1989; Clore and Gronenborn, 1991), and residual dipolar coupling restraints derived from the partially ordered proteins dissolved in an anisotropic media (Tjandra et al., 1996; Tjandra and Bax, 1997; Clore et al., 1998). Among these, NOE restraints are essential for defining the structure to high resolution. Specifically, NOE restraints are obtained from 3D $^{15}N$-edited (Marion et al., 1989a; Zuiderweg and Fesik, 1989), $^{13}C$-edited (Muhandiram et al., 1993), or 3D or 4D $^{15}N$- and $^{13}C$-edited NOESY experiments (Kay et al., 1990; Farmer II, 1991). TROSY-based NOESY experiments (Pervushin et al., 1999, 2000; Zhu et al. 1999; Nocek et al., 2000; Xia et al., 2000; Meissner and Sørensen, 2000a, b; Brutscher et al., 2001) have been shown to be superior in signal enhancement for $^{15}N$-, $^{13}C$- and $^2H$-labeled large proteins. For medium-sized proteins (Mw $<$ 20 kDa), traditional isotope-edited NOESY experiments remain the preferred choice. With a suite of multidimensional and multinuclear NMR experiments well established and driven by the possibility of genome scale proteome analyses, there is a continued need for rapidly solving the structures of a large number of proteins (Anonymous, 1998; Šali, 1998; Brenner, 2001). To

*To whom correspondence should be addressed. E-mail: xgao@mail.uh.edu

achieve this goal, improvement in the efficiency of NMR data collection is of particularly importance.

Simultaneous data acquisition in time-sharing (TS) multi-dimensional NMR experiments has been demonstrated to effectively reduce experiment time by as much as a factor of two. In these experiments, $^{1}$H NOEs are simultaneously spin-labeled with $^{15}$N and $^{13}$C frequencies during one of the evolution time periods. Spectral data processing allows the separation of $^{13}$C-correlated from $^{15}$N-correlated peaks to give two spectra from one NMR experiment. Several types of TS 2D, 3D and 4D experiments have been reported (Pascal et al., 1994; Farmer and Mueller, 1994; Vis et al., 1994; Sattler et al., 1995; Jerala and Rule, 1995, Xia et al., 2001). Among these, TS $^{15}$N- and $^{13}$C-edited NOESY-HSQC experiments have become increasingly important as two sets of NOE data the $^{15}$N-edited NOE and $^{13}$C-edited NOE data, can be simultaneously extracted in a single experiment to allow interproton distance assignments. However, in these experiments ambiguous assignments exist since all types of $^{1}$H are displayed in the $F_1$ dimension (all $^{1}H \rightarrow F_1$, $^{13}$C and $^{15}N \rightarrow F_2$, $^{1}H_C$ and $^{1}H_N \rightarrow F_3$) (Pascal et al., 1994; Vis et al., 1994; Sattler et al., 1995) and exhibit rather crowded cross peaks in some spectral region. 4D NOESY experiments may be used to resolve these ambiguous assignments, but data collection would take days of instrument time and the spectral resolutions are significantly penalized. A set of NMR data, 3D N-N-H, C-C-H, C-N-H and N-C-H HSQC-NOESY-HSQC collected in separate experiments (Zhang and Forman-Kay, 1997; Diercks et al., 1999) in combination with 3D H-CN-H NOESY-HSQC, provides an alternative strategy for the lengthy 4D experiments. Further gain can be attained if the four 3D (N-N-H, C-C-H, C-N-H and N-C-H HSQC-NOESY-HSQC) spectra could be acquired in one experiment with simultaneous acquisition strategy.

In this work, the 2D TS CN-H HSQC (Pascal et al., 1994; Vis et al., 1994) is optimized by combining the advantageous features of several TS experiments reported in the literature. The TS pulse scheme is incorporated into 3D TS experiments as a basic building block to simultaneously obtain isotope-edited NOESY spectra. Based on these results, a new $^{13}$C- and $^{15}$N-edited 3D double time-sharing (2TS) CN-CN-H HSQC-NOESY-HSQC experiment is developed using a scheme to spin label $^{1}$H NOE simultaneously with $^{13}$C and $^{15}$N frequencies in both $t_1$ and $t_2$ dimensions (therefore, termed 2TS). This single experiment produces four 3D spectra as discussed above and total $^{1}H_C$ and $^{1}H_N$ NOE correlations in a protein. This 2TS experiment and the improved versions of the existing 2D TS CN-H HSQC and 3D TS H-CN-H NOESY-HSQC demonstrate better performances in water suppression, sensitivity, and digital resolution in the $^{15}$N dimension for a $^{15}$N- and $^{13}$C-labeled protein sample dissolved in $H_2O$.

## Materials and experiments

A uniformly $^{13}$C and $^{15}$N-labeled protein sample, tm1112 (1.0 mM, 89 amino acids with a His-tag, 10.7 kDa, in 450 mM NaCl, 25 mM $Na_2HPO_4$, 10 mM DTT, 20 μM $Zn^{2+}$, 1 mM benzamidine, 1× inhibitor mixture, 0.01% $NaN_3$, pH 6.5, $H_2O/D_2O$-95%/5%), from the protein structure production pipeline of the Northeast Structure Genomics Consortium (http://www.nesg.org) was used. The assignments of the $^{1}$H, $^{13}$C and $^{15}$N resonances have been made in a separate study (Y. Xia et al., unpublished results). NMR data sets in this work were recorded at 25 °C using a Bruker Avance 600 MHz NMR spectrometer. All data were processed using NMRPIPE (Delaglio et al., 1995). No filter for water suppression in data processing was used to avoid distortions of the spectra in the $^{1}H_\alpha$ region. Detailed description of water suppression is provided in Results and Discussion.

The 2D TS CN-H HSQC pulse scheme used in this work is shown in Figure 1A and the experimental parameters are specified in the figure legend. In a separate experiment, an alternative version of 2D TS CN-H HSQC was used for comparison purposes and the used delays between pulses are the same as that in (Figure 1d by Sattler et al. (1995). These experiments used same or comparable parameters; 32 × 1024 data matrices in complex data points in the time domain were acquired with 16 transients for each FID. The spectral widths of $^{13}$C and $^{15}$N in $F_1$ dimension were 3621 Hz ($sw_1^C$) and 1508 Hz ($sw_1^N$), respectively. Linear prediction to 128 complex points in the $t_1$ dimension and cosine square bell window functions in the $t_1$ and $t_2$ dimensions were used before Fourier transformation and the final spectrum contains 256 × 1024 data points.

For 3D 2TS CN-CN-H NOESY shown in Figure 1B, the data matrix in the time domain was composed of 70 × 32 × 1024 complex points, with spectral widths of $sw_1^C = 9958$ Hz, $sw_1^N = 1508$ Hz, $sw_2^C = 3621$ Hz, $sw_2^N = 1508$ Hz, and

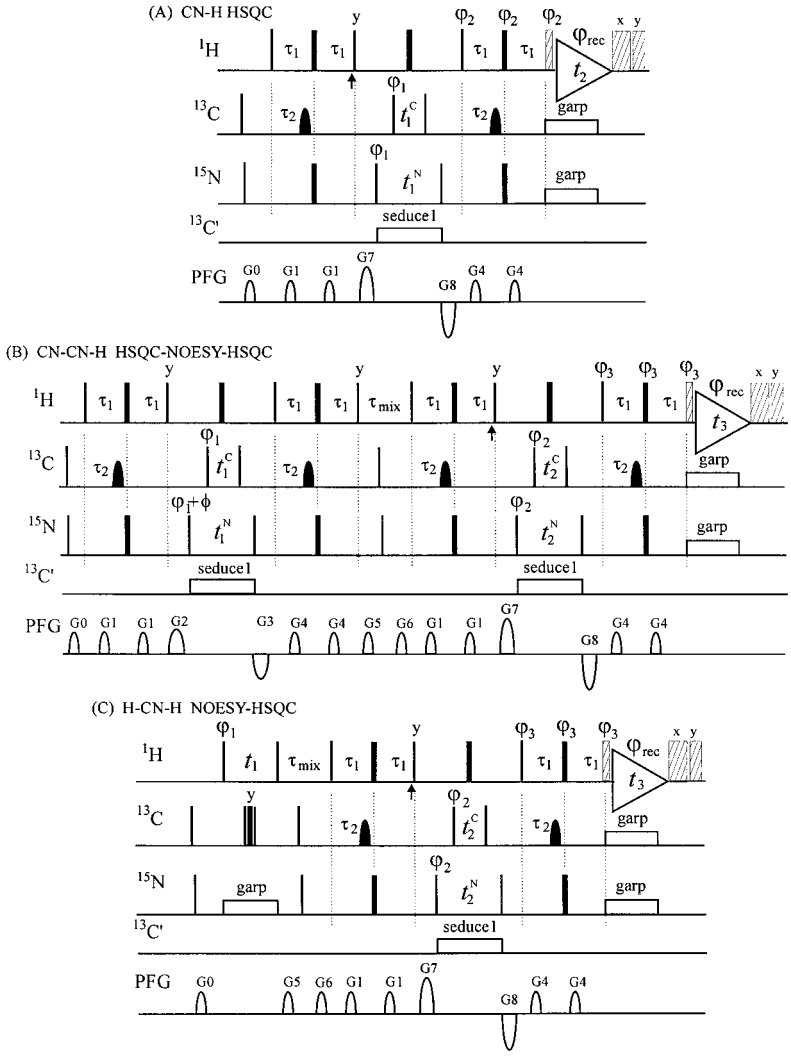


*Figure 1.* Pulse sequences of $^{15}$N and $^{13}$C-separated HSQC and NOESY experiments. Narrow and wide bars represent 90° and 180° pulses, respectively. The spin lock pulse (1 ms) and x and y purge pulses (3 and 2 ms) with 25 W of radio frequency power are applied immediately before and after acquisition, respectively (caution: do not use too high power level that will cause probe damage). The carrier frequencies of $^{1}$H, $^{15}$N, $^{13}$C and $^{13}$CO were centered at 4.7, 120, 38 and 174 ppm, respectively. The $^{13}$C shape pulses are 200 μs G3 180° pulses (Emsley and Bodenhausen, 1987), which are used to filter out the aromatic carbon resonances. If the aromatic resonances are expected to be involved in carbon dimensions, the $^{13}$C carrier and its spectral width can be adjusted so that cross peaks to aromatic protons are folded an odd number of times and therefore appear 180° out of phase relative to cross peaks to NH (Pascal et al., 1994) in addition to that the $^{13}$C shape pulses are replaced by adiabatic inversion 180° (Kupce and Freeman, 1995) or hard 180° pulses. $^{13}$C and $^{15}$N decoupling used garp sequences (Shaka et al., 1985). $^{13}$CO was decoupled with respect to $^{15}$N and $^{13}$C$^{\alpha}$ with a cosine-modulated seduce1 decoupling sequences (McCoy and Mueller, 1992a, b), the 90° pulse width is 250 μs and the modulation frequency is 20400 Hz, which is the frequency difference between 174 ppm (the center of $^{13}$CO resonances) and 38 ppm (the carrier of $^{13}$C channel). $\tau_1 = 2.2$ ms, $\tau_2 = 1.6$ ms, $\tau_{mix} = 150$ ms. Recovery delays between two scans were set to 1.0 s. For $^{13}$C and $^{15}$N simultaneous evolution times, $t_1^C$ and $t_1^N$ of (A) and $t_2^C$ and $t_2^N$ of (B) and (C), half point delays (Bax et al., 1990) were used. The durations and strengths of the gradients are G0 = (1 ms, 15 G cm$^{-1}$); G1 = (0.5 ms, 5 G cm$^{-1}$); G2 = (1 ms, 8 G cm$^{-1}$); G3 = (1 ms, −20 G cm$^{-1}$); G4 = (1 ms, 6 G cm$^{-1}$), G5 = (1 ms, 5 G cm$^{-1}$), G6 = (1 ms, 10 G cm$^{-1}$), G7 = (3 ms, 25 G cm$^{-1}$), and G8 = (4 ms, −25 G cm$^{-1}$). Water suppression can be further improved by adding another 1 ms of spin lock pulse with phase x at time arrow points to. Default phases were x. (A) 2D TS CN-H HSQC: $\varphi_1$ = (x, −x); $\varphi_2$ = (x, x, y, y, −x, −x, −y, −y); $\varphi_r$ =(x, −x, y, −y, −x, x, −y, y). Quadrature detections in $t_1^C$ and $t_1^N$ were acquired via States-TPPI (Marion et al., 1989b) of $\varphi_1$. (B) 3D 2TS CN-CN-H NOESY: $\varphi_1$ = (x, −x); $\varphi_2$ = (x, x, −x, −x); $\varphi_3$ = (x, x, x, x, y, y, y, y, −x, −x, −x, −x, −y, −y, −y, −y); $\varphi_r$=(x, −x, −x, x, y, −y, −y, y, −x, x, x, −x, −y, y, y, −y). Quadrature detections in $t_1^C$, $t_1^N$, $t_2^C$ and $t_2^N$ were acquired via States-TPPI of $\varphi_1$ and $\varphi_2$. $\phi = 0°$ is for ($^{13}$C+$^{15}$N) signals and $\phi = 180°$ is for ($^{13}$C-$^{15}$N) signals and these FIDs were acquired in an interleave mode and stored separately. Eight FIDs were collected for each ($t_1$ and $t_2$) time set. An AU program, proc_cnnoesy, was created to split the data into two 3D spectra. (C) 3D TS H-CN-H NOESY: phase cyclings are the same as those in (B). Quadrature detections in $t_1$, $t_2^C$ and $t_2^N$ were acquired via States-TPPI of $\varphi_1$ and $\varphi_2$.

$sw_3 = 8389$ Hz, respectively. For the 3D TS H-CN-H NOESY experiment shown in Figure 1C, the data matrix in the time domain was composed of $100 \times 32 \times 1024$ complex points, with spectral widths of $sw_1 = 6000$ Hz, $sw_2^C = 3621$ Hz, $sw_2^N = 1508$ Hz and $sw_3 = 8389$ Hz, respectively. These experiments used 16 transients for each fid. Linear predictions to 64 complex points in the $t_2$ dimension and cosine square bell window functions in the $t_1$, $t_2$ and $t_3$ dimensions were used before Fourier transformation and the final spectra contain $256 \times 128 \times 1024$ data points.

## Results and discussion

### *General description of the methods*

*Improved 2D TS CN-H HSQC as a basic building block for advanced 3D TS experiments.* The pulse sequence of a 2D TS CN-H HSQC experiment, modified and optimized based on reports in the literature (Pascal et al., 1994; Boelens et al., 1994), is depicted in Figure 1A. The 2D TS CN-H HSQC pulse scheme contains a core double INEPT for simultaneous polarization transfers and water suppression pulses to assist data acquisition of a protein sample in $H_2O$. This experiment generates correlations of $^{13}C$ with its attached aliphatic proton ($^1H_C$) and $^{15}N$ with its attached amide proton ($^1H_N$), respectively. Therefore, two HSQC spectra, C-H HSQC and N-H HSQC, are simultaneously obtained in a single experiment. In the reported 2D TS HSQC experiments (Boelens et al., 1994), a moderate presaturation irradiation and a spin lock pulse were applied for water suppression, resulting in reduction in signal intensities of $^1H_N$ and $^1H_\alpha$ resonances close to the water peak. In addition, in this experiment, the absence of $^{13}CO$-decoupling results in fast decay of the signals of $^{15}N$ and $^{13}C_\alpha$. In the 3D TS NOESY-HSQC (H-CN-H) experiment (Pascal et al., 1994) , the digital resolution of $^{15}N$ and the water suppression effect were also not optimal, although during this work, the authors were brought to attention of a new version of the pulse scheme with optimized $^{15}N$ digital resolution used internally in the Kay's laboratory. The pulse scheme shown in Figure 1A is designed to improve upon these shortcomings: two strong gradient pulses (G7 and G8, Figure 1A) flanking $t_1^C$ and $t_1^N$ with opposite polarities, the purge pulses immediately after acquisition (Pascal et al., 1994), and spin lock just before acquisition (Boelens et al., 1994) are used in combination to improve water suppression; suitable evolution times for $^{13}C$ or $^{15}N$ (Boelens et al., 1994) are employed to maintain the digital resolution of $^{15}N$ whose signals are acquired within a narrower spectral window than that of $^{13}C$; a cosine-modulated seduce1 $^{13}CO$-decoupling scheme (McCoy and Mueller, 1992a,b) is applied to decouple $^{13}CO$ from both $^{15}N$ and $^{13}C_\alpha$ resonances.

*3D 2TS experiment.* The important gain from the reported TS experiments is reduced time because two spectra are obtained from a single experiment, ideally without sacrificing spectral resolution. The pulse sequence of our new 3D 2TS CN-CN-H HSQC-NOESY-HSQC experiment is depicted in Figure 1B. In this scheme, the improved 2D TS CN-H HSQC pulse sequence (Figure 1A) is applied as the building block before and after mixing time $\tau_{mix}$. $^{13}C$- and $^{15}N$-edited NOE peaks can be easily distinguished in the $F_2$ dimension because the $^1H_C$ and $^1H_N$ resonances in $F_3$ dimension are located in different spectral regions except for aromatic protons. The $^{13}C$- and $^{15}N$-related peaks are deconvoluted by recording two sets of FIDs for each $t_1$ and $t_2$ time set (Farmer II and Mueller, 1994). This is accomplished in 3D 2TS CN-CN-H HSQC-NOESY-HSQC by setting additional phase $\phi = 0°$ and 180° for ($^{13}C + {}^{15}N$) and ($^{13}C - {}^{15}N$) signals, respectively. Therefore, after addition and subtraction of the two sets of FIDs recorded, there are effectively two sets of 3D TS data generated using the time for a single 3D experiment. In order to reduce artifacts from subtraction of the two 3D spectra, the FIDs with $\phi = 0°$ and 180° are acquired interleavely (Farmer and Mueller, 1994). The two sets of 3D TS data contain resolved $^{13}C$ and $^{15}N$ in $F_1$ and are equivalent of 3D TS N-CN-H and C-CN-H HSQC-NOESY-HSQC and their sensitivities are enhanced by $\sqrt{2}$ times due to the addition and subtraction of two sets of 3D data in the 3D 2TS HSQC-NOESY-HSQC. Fourier transforms of the two 3D TS NMR data sets produce four 3D NOESY spectra, which reflect the full NOE connectivities of $^1H_C \leftrightarrow {}^1H_C$, $^1H_C \leftrightarrow {}^1H_N$, $^1H_N \leftrightarrow {}^1H_C$, and $^1H_N \leftrightarrow {}^1H_N$. Therefore, four 3D spectra, 3D C-C-H, 3D C-N-H, 3D N-C-H, and 3D N-N-H HSQC-NOESY-HSQC, are simultaneously obtained with the 3D 2TS CN-CN-H HSQC-NOESY-HSQC experiment. The experimental time required for acquiring a 3D 2TS CN-CN-H HSQC-NOESY-HSQC is only $\frac{1}{4}$th of that needed in conventional experiments without additional loss of signal sensitivity or spectral resolution.

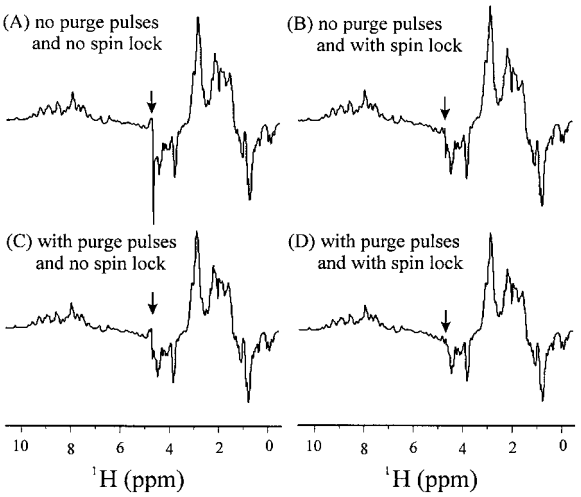


*Figure 2.* Comparisons of the water suppression schemes in 2D CN-H HSQC experiments. The four 1D spectra are from the first FIDs of 2D CN-H HSQC experiments with same conditions except that for spectrum: (A) The purge pulses were removed and the spin lock pulse was replaced by a hard 90° pulse; (B) the purge pulses were removed but the spin lock pulse remained; (C) the purge pulses remained but the spin lock pulse was replaced by a hard 90° pulse; (D) both the purge pulses and spin lock pulse remained. The arrows point to water peaks. Negative $^1H_C$ peaks means that the $^1H_C$-attached carbon resonances are folded back due to half-point delay used in the pulse sequence.

*Improved 3D H-CN-H experiment.* The improved 2D TS HSQC pulse sequence is also applied to enhance the previously reported 3D TS H-CN-H NOESY-HSQC experiment (Figure 1C) (Pascal et al., 1994; Vis et al., 1994). From this experiment, two 3D spectra, 3D $^{13}$C- and $^{15}$N-separated H-C-H and H-N-H NOESY-HSQC spectra, can be obtained. The experimental time for this experiment is half of that using conventional data acquisition approach. The three improvements discussed above for the new 3D 2TS CN-CN-H HSQC-NOESY-HSQC experiment, water suppression pulses, different evolution times for $^{15}$N and $^{13}$C, and $^{13}$CO decoupling, were implemented. When used in combination, the resulting spectra exhibit improved quality.

*Experimental results*

*Water suppression spectra.* Comparisons of several water suppression pulse schemes to be used for the 2D and 3D TS NMR experiments indicate that combined use of spin lock and purge pulses before and after acquisition, respectively, gives best water suppression results. The water suppression effects of the pulse schemes compared are shown in Figure 2. The 1D spectra plotted are from the first FID of 2D TS CN-H HSQC experiments using the specified water suppression method, and thus bear direct relevance to the water suppression quality in the 2D experiment. Inspections of the four spectra in Figure 2, in which the effect of purge and spin lock pulses is seen when they are used alone or in combination, indicate that the water suppression with both purge and spin lock pulses gives the most satisfactory effect, although there is about a 7% or 8% reduction of sensitivity compared to the spectrum shown in Figures 2B or 2C. These effects are additive; therefore, using both spin lock and purge pulses results in an overall ∼15% reduction of sensitivity (Figures 2A and 2D). This loss in signal intensity in exchange for improved water suppression is considered to be worthwhile. The water suppression scheme used in Figure 1D with combined use of spin lock and purge pulses are thus used in the 2D and 3D TS experiments described below. If full gain in sensitivity is desirable, either the purge pulses can be removed or spin lock pulse can be replaced by a hard 90° $^1$H pulse.

*Spectral comparison with and without $^{13}$CO decoupling.* Seduce1 $^{13}$CO-decoupling eliminates signal decay of the $^{15}$N-$^1H_N$ and $^{13}C_\alpha$-$^1H_\alpha$ correlations due to $^1J_{NCO}$ and $^1J_{CACO}$. Two 2D TS data sets were collected: one is 2D TS CN-H HSQC (Figure 3A) with seduce1 $^{13}$CO-decoupling (pulse scheme shown in Figure 1A) and the other is the same experiment except without the seduce1-decoupling (data not shown). Without using $^{13}$CO decoupling the spectrum shows 22% and 41% reductions in signal intensities compared to that using $^{13}$CO decoupling for the $^{15}$N-$^1H_N$ and $^{13}C_\alpha$-$^1H_\alpha$ correlations, respectively. There is no evident effect on other correlations with CO-decoupling.

*Spectral comparison using the INEPT or the echo/antiecho scheme.* The double INEPT scheme is more sensitive than the double echo/antiecho scheme for magnetization transfer in the TS experiments. Figure 3B displays a 2D spectrum acquired based on an alternative version of 2D TS HSQC (Figure 1d in Sattler et al., 1995) with the inclusion of seduce1 $^{13}$CO-decoupling pulses. Figure 3B is compared with a similar experiment (Figure 3A) using the double INEPT rather than the double echo/antiecho scheme after the TS evolution. Figure 3C shows 1D trajectories from the spectra shown in Figure 3A (slices a1 and a2) and 3B (slices b1 and b2) to provide a semi-

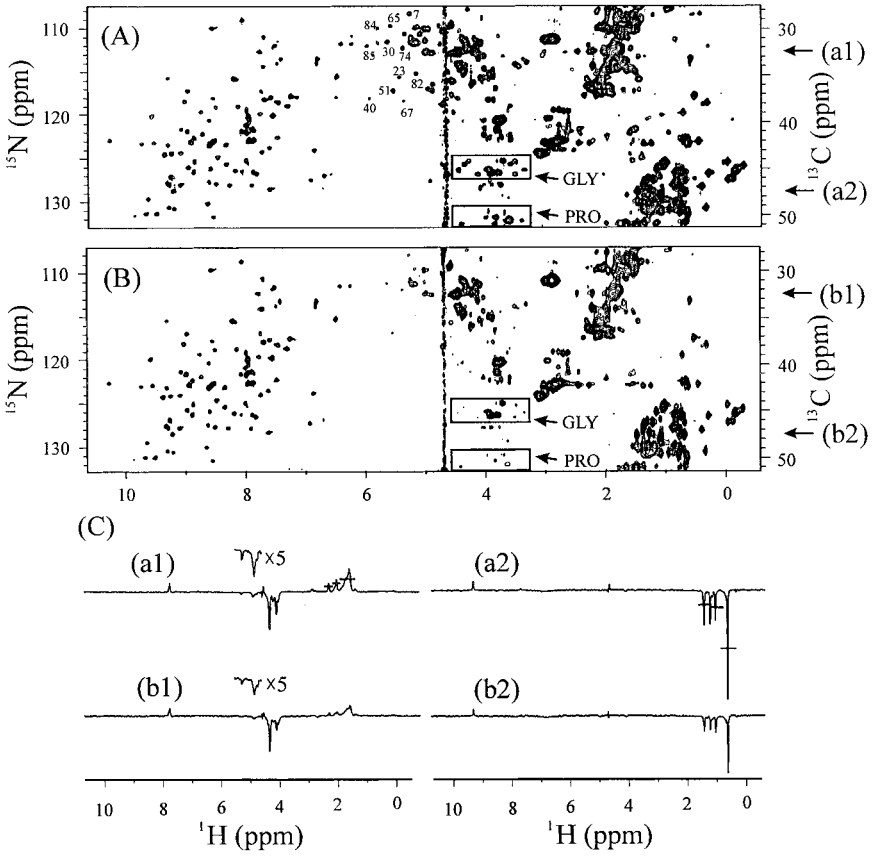


*Figure 3.* Comparisons of the spectra of 2D TS CN-H HSQC of (A) this work and (B) the literature (Sattler et al., 1995). Identical data acquisition and processing parameters were used. In (A) the correlations of $C^{\alpha}$-$H^{\alpha}$ of selected residues close to the water signal were indicated by their residue numbers; the peaks in boxes designed with GLY and PRO were from the correlations of $C^{\alpha}$-$H^{\alpha}$ of GLY residues and $C^{\delta}$-$H^{\delta}$ of PRO residues, respectively. (C) 1D traces (a1, a2, b1, and b2) taken from the 2D spectra shown in (A) and (B) at the positions indicated by arrows. The horizontal short bars in the spectra of (a1) and (a2) indicate the heights of corresponding peaks in (b1) and (b2).

quantitative comparison of the signal intensities. For the peaks marked with a horizontal bar in Figure 3C, the ratio of the two sets of data (a1/b1 and a2/b2, Figure 3C) is about 2-fold, showing the first experiment (this work) twice as sensitive compared to the alternative version. Data analysis after normalization indicates that, on average, the sensitivity enhancement of the $^{15}$N-$^{1}$H$_N$ and $^{13}$C-$^{1}$H$_C$ cross peaks in the spectra using the double INEPT pulses (Figure 3A) ranges from 14 to 120%, respectively. $CH_2$ groups are not expected to have increased sensitivity in the echo/antiecho transfer. For instance, the majority of peaks marked with residue number and peaks in boxes belonging to glycine and proline residues in Figure 3A disappeared in Figure 3B due to sensitivity reduction caused by the echo/antiecho scheme. These peaks were from the correlations of $C^{\alpha}$-$H^{\alpha}$ of the glycine residues and $C^{\delta}$-$H^{\delta}$ of the proline residues, respectively. The corresponding carbons exhibit shorter transverse relaxation time constants since they are connected to two hydrogens, and thus they are more sensitive to the extra delays used in the echo/antiecho scheme.

Further analysis indicates that although the echo/antiecho scheme used in 2D TS CN-H HSQC type of experiments (Sattler et al., 1995) can improve the water suppression, it considerably reduces signal strength of $^{13}$C (Figure 3B) or $^{15}$N. This scheme when used for coherence transfer from $^{15}$N to $^{1}$H$_N$ in constant-time-type experiments (see Figure 7.27, in Cavanagh, 1996) with selective gradient field applied in the constant-time period may enhance signal intensities by ~20% ($\sqrt{2}$ theoretically) for small proteins. However, this increase in signal intensity is canceled due to extra delays required in the echo/antiecho scheme compared with a simple INEPT in a routine 2D $^{15}$N-$^{1}$H HSQC. For the 2D $^{1}$H,$^{13}$C-HSQC part

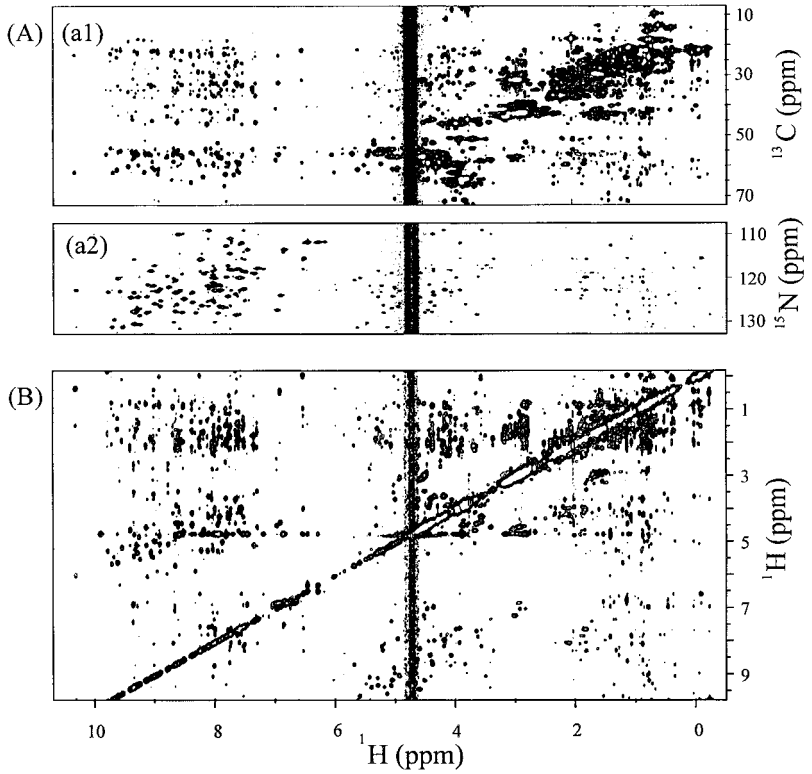


*Figure 4.* (A) Projections of the 3D 2TS CN-CN-H HSQC-NOESY-HSQC spectrum along the $F_2$ dimension: (a1) 3D C-CN-H HSQC-NOESY-HSQC. Left spectral region from ~6.7 ppm contains $(^1H_C)^{13}C$-$^{15}N$-$^1H_N$ NOE correlations and right spectral region from ~6.7 ppm contains $(^1H_C)^{13}C$-$^{13}C$-$^1H_C$ NOE correlations. (a2) 3D N-CN-H HSQC-NOESY-HSQC. Left spectral region from ~6.7 ppm contains $(^1H_N)^{15}N$ -$^{15}N$-$^1H_N$ NOE correlations and right spectral region from ~6.7 ppm contains $(^1H_N)^{15}N$-$^{13}C$-$^1H_C$ NOE correlations. (B) Projection of the 3D TS H-CN-H NOESY-HSQC spectrum along the $F_2$ dimension. Left spectral region from ~6.7 ppm contains $^1H_{all}$-$^{15}N$-$^1H_C$ NOE correlations and right spectral region from ~6.7 ppm contains $^1H_{all}$-$^{13}C$-$^1H_N$ NOE correlations.

(Sattler et al., 1995), the applied echo/antiecho scheme considerably reduces signal intensities due to the fast transverse relaxation of $^{13}C$ and $^1H_C$ during the interval delays, which are set to compromise the differences in coherence transfers of CH, $CH_2$ and $CH_3$ groups. For large proteins with long overall rotational correlation times, which correlates the transverse relaxation decays during the extra delays, the signal decays become more apparent. The lower sensitivity shown in the spectral comparison in Figure 3B may also because the many pulses used (Sattler et al., 1995) which render the experiment sensitive to mis-setting of the pulse lengths.

*3D 2TS CN-CN-H HSQC-NOESY-HSQC.* 3D 2TS CN-CN-H HSQC-NOESY-HSQC spectra were acquired using the pulse sequence shown in Figure 1B. The 3D spectra derived from this experiment are shown in Figures 4A and 5A, demonstrating that using a single 3D experiment, two 3D TS data sets are extracted by adding and subtracting FIDs. These are 3D C-CN-H and 3D N-CN-H spectra, respectively. Further, from each of the two 3D 2TS data set (Figure 4A), two 3D NOESY data sets are resolved, which contain (a1) $(^1H_C)^{13}C$-$^1H_N$, (a2) $(^1H_C)^{13}C$-$^1H_C$, (a3) $(^1H_N)^{15}N$-$^1H_N$, and (a4) $(^1H_N)^{15}N$-$^1H_C$ NOE correlations (Figure 5A). As an illustration, the assignments of the NOE cross peaks involving T52 HN, T67 HB, and T40 HG2# are indicated in Figure 5A. Therefore, the new 3D 2TS experiment shortens experimental time by simultaneously acquiring four sets of 3D data and improves the efficiency of 3D TS experiment by a factor of two. It is noted that the water suppression of 3D 2TS CN-CN-H HSQC-NOESY-HSQC is not as good as that of the 2D CN-H HSQC experiment. This may be due to extended experiment time needed for the 3D experiment while optimization was based on first FID at the beginning of the experiment. Water suppression can be further improved by adding an-

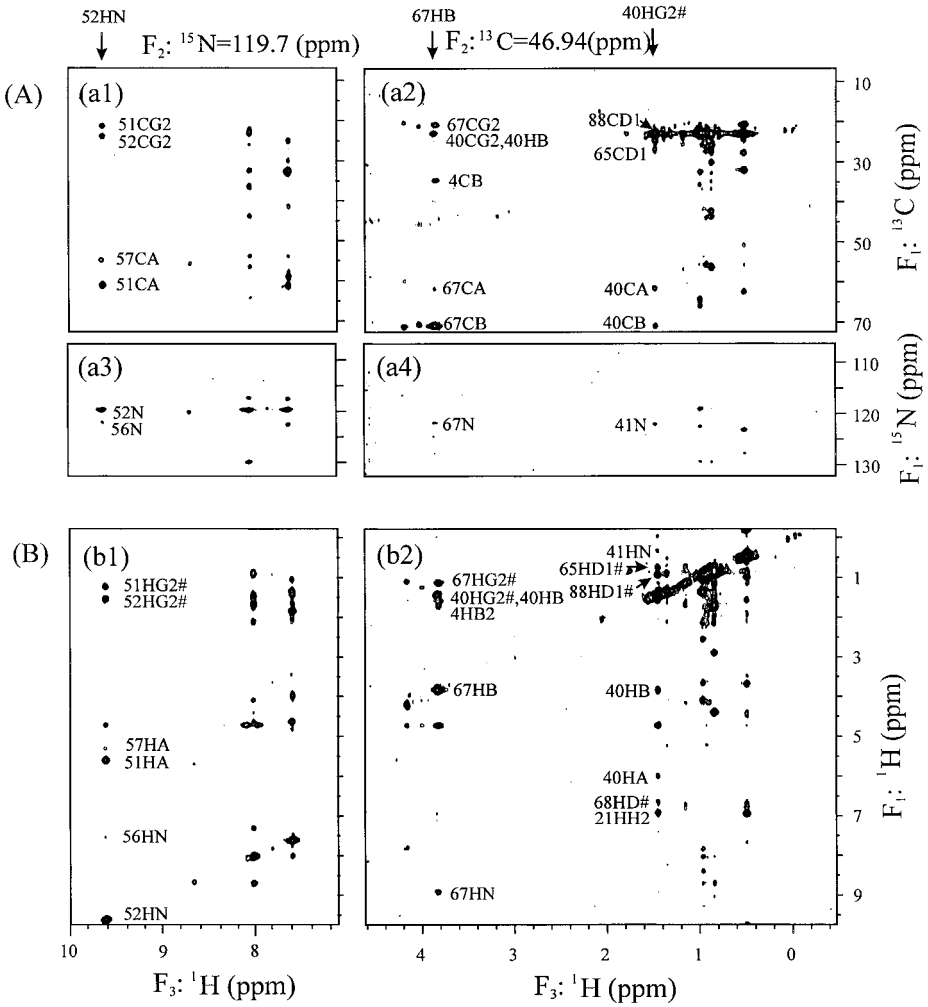


*Figure 5.* Expanded 2D planes of the 3D 2TS and TS spectra. (A) 2D planes derived from 3D 2TS CN-CN-H HSQC-NOESY-HSQC showing: (a1) $(^1H_C)^{13}C$-$^1H_N$, (a2) $(^1H_C)^{13}C$-$^1H_C$, (a3) $(^1H_N)^{15}N$-$^1H_N$ and (a4) $(^1H_N)^{15}N$-$^1H_C$ NOE correlations. (B) 2D planes of 3D TS H-CN-H NOESY-HSQC showing; (b1) $^1H_{all}$–$^1H_N$ and (b2) $^1H_{all}$-$^1H_C$ NOE correlations. (a1), (a3), and (b1) planes are selected at $^{15}N = 119.7$ ppm (the assignment for HN of T52 is indicated); (a2), (a4), and (b2) planes are selected at $^{13}C = 46.94$ ppm (the assignment for CB of T67 at 70.97 ppm and CG of T40 at 22.94 ppm are indicated).

other 1 ms of spin lock pulse with phase x at time arrow points to Figure 1.

The spectrum of an improved version of 3D TS H-CN-H NOESY-HSQC was acquired according to the pulse sequence shown in Figure 1C. The projection of the spectrum is displayed in Figure 4B. Two 3D data sets are resolved from this single experiment, which contain H-N-H ($^1H_{all}$-$^1H_N$) and H-C-H ($^1H_{all}$-$^1H_C$) NOE correlations (Figure 5B). In comparison, the spectra of the four 3D data sets derived from the 3D 2TS experiment are consistent with these derived from 3D TS H-CN-H experiment (Figures 4 and 5).

The new 3D 2TS HSQC-NOESY-HSQC adds additional power of spectral resolution when used in combination with 3D TS NOESY-HSQC, reducing ambiguities and errors in its spectral assignments. For spin moieties, X-$^1H_X$ and Y-$^1H_Y$ (X, Y = $^{13}C$ or $^{15}N$), in 3D 2TS CN-CN-H HSQC-NOESY-HSQC, the NOE mixing pattern for isotope-edited $^1H$ resonance is: $^1H_X$ $\underline{X}$ $^1H_X$ $\xrightarrow{\text{NOE mixing}}$ $^1H_Y$ $\underline{Y}$ $^1\underline{H}_Y$, and in 3D TS H-CN-H NOESY-HSQC, the NOE mixing pattern is: $^1\underline{H}_X$ $\xrightarrow{\text{NOE mixing}}$ $^1H_Y$ $\underline{Y}$ $^1\underline{H}_Y$ where the underlined nuclei are frequency-labeled. The new 3D 2TS experiment offers an alternative by linking NOEs to $^{13}C$ and $^{15}N$ nuclei rather than to $^1H$ in $F_1$ in the 3D TS exper-

iment (Figures 4 and 5). In contrast to 3D TS NOESY projection (Figure 4B), the diagonal is absent in the regions of $^1H_N$-$^{13}C(^1H_C)$ and $^1H_C$-$^{15}N(^1H_N)$ of 3D 2TS HSQC-NOESY-HSQC projection (Figure 4A). The combination of the two 3D experiments provides four chemical shifts (pseudo 4D connectivities) for the assignments of the corresponding NOE cross peaks. Ambiguous assignments may be resolved if three of the four chemical shifts can be resolved.

The 3D 2TS CN-CN-H and 3D TS H-CN-H spectra are complementary data sets which provide critical information for unambiguously, more completely assigning NOE cross peaks for a large protein in $H_2O$. In Figure 5, expanded 2D planes are plotted with $^{15}N$ = 119.70 ppm (Figures 5A (a1 and a3) and 5B (b1) and $^{13}C$ = 46.94 ppm (note that $F_2$ $^{13}C$ dimension has a width of 24 ppm and is folded) and the corresponding assignments are 52N (119.70 ppm), 67CB (70.94 ppm) and 40CG (22.94 ppm). Accordingly, three $^1H$ resonances in the $F_3$ dimension (x-axis) are assigned to the indicated $^{13}C$ and $^{15}N$ resonances, which are 52HN (9.63 ppm), 67HB (3.85 ppm) and 40HG2# (1.46 ppm) (Figure 5A (a1 and a2)). However, further NOE assignments in the $F_1$ dimension (y-axis, Figure 5) can be ambiguous. For instance, for the peak ($F_3$ = 40HG2# and $F_1$ = 0.78 ppm) in Figure 5B (b2), there were four possible $^1H$ assignments, which are 23HG2# (0.77 ppm), 44HD1# (0.78 ppm), 65HD1# (0.78 ppm), and 66HG1# (0.78 ppm), giving rise to possible overlapping peaks in 3D TS H-CN-H spectra. At the $^{13}C$ frequency, these $^1H$ resonances have been assigned to correlate with 17.80, 25.71, 26.87, and 22.38 ppm, respectively (Xia et al., unpublished results). These $^{13}C$ related cross peaks are resolved in the 3D 2TS CN-CN-H spectra. Since only the peak with its $^{13}C$ chemical shift = 26.87 ppm appears in the $F_1$ dimension of Figure 5A (a2), the cross peak in Figure 5B (b2) can then be unambiguously assigned to a long range NOE connecting 65HD1# (0.78 ppm) with 40HG2# (1.46 ppm), excluding three other possible $^1H$ assignments. Another example is the assignment of the peak ($F_3$ = 56HN and $F_1$ = 9.63 ppm) in Figure 5B (b1). There were three possible $^1H$ assignments: 17HN (7.59 ppm), 20HN (7.55 ppm) and 56HN (7.56 ppm), giving rise to possible overlapping peaks in 3D TS H-CN-H spectra. These amide protons correlate with $^{15}N$ at 111.50, 118.13, and 122.23 ppm, respectively (Y. Xia et al., unpublished results). These $^{15}N$ related cross peaks are resolved in the 3D 2TS CN-CN-H spectra. Since only the peak with its $^{15}N$ chemical shift = 122.23 ppm appears in the $F_1$ dimension of Figure 5A (a1), the $^1H$-$^1H$ cross peak in Figure 5B (b1) can then be unambiguously assigned to an NOE connecting 56HN (7.56 ppm) with 52HN (9.63 ppm), excluding the other two possible $^1H$ assignments. Long range NOEs are especially valuable information for structure elucidation.

It is useful to compare the sensitivity of the new 3D 2TS CN-CN-H HSQC-NOESY-HSQC with the 3D TS H-CN-H NOESY-HSQC and with the conventional practice of using HMQC-NOESY experiments. Compared with the TS experiment, the 2TS experiment uses two more double INEPT blocks in the $F_1$ dimension (Figures 1B and 1C) where each double INEPT uses $2\tau_1$ = 4.4 ms. Therefore, the sensitivity of the first FID in 2TS experiment is 70% of that of the TS experiment. However the two derived 3D TS spectra from the 3D 2TS experiment, 3D TS C-CN-H and N-CN-H, are obtained through addition or subtraction of the 3D data, and thus the sensitivities of these spectra are in fact about one, $0.7 \times \sqrt{2} = 0.98$, comparable to that of 3D TS H-CN-H NOESY-HSQC. For a larger protein, such as a 20 kDa protein, $T_2^*(^1H)$ is shorter ($\sim$15 ms), the estimated sensitivities of the derived 3D TS C-CN-H and N-CN-H in the 3D 2TS CN-CN-H become 80% [$\exp(-4\tau_1/15) \times \sqrt{2} \approx 0.8$] of that of 3D TS H-CN-H NOESY-HSQC. In this case, useful 3D 2TS spectra can be expected within a reasonable experimental time. When the 3D 2TS CN-CN-H HSQC-NOESY-HSQC experiment compared with that using conventional $D_2O$ 3D NOESY-HMQC and $H_2O$ 3D NOESY-HMQC in combination, the overall intensity is to certain degree compromised. The use of double INEPT with a delay of 4.4 ms ($2\tau_1$) is less ideal for both $^1H_C$, $^{13}C$ and $^1H_N$, $^{15}N$ magnetization transfers since this is a longer relaxation decay for $^1H_C$ than that of 3.4 ms used in HMQC experiments. Additionally, the greater number of 90° and 180° pulses used in the 3D 2TS experiment have off-resonance effect which contributes to signal reduction, affecting observation of weak NOE signals. For a sensitive 3D 2TS experiment, higher concentration of sample would be needed. Therefore, one has to balance the considerations of various factors, such as affordable time and sample concentrations, in the selection of experimental methods.

## Conclusions

The 3D 2TS NOESY experiment reported here is to further explore the advantages of simultaneous data acquisition to shorten the time for NMR data collection and attain accurate interproton NOE assignments. Furthermore, efforts were made to improve the existing TS NOESY and TS HSQC experiments in water suppression, spectral digital resolution, and sensitivity. 2D TS HSQC experiments have been extensively discussed in the literature (Boelens et al., 1994; Sattler et al., 1995), but there are improvements remaining to be made. As shown in Figure 2, best water suppression effect was obtained by combining the purge pulses and spin lock. Since in this work the spectral widths of $^{13}C$ and $^{15}N$ were set differently, the digital resolutions in both $^{13}C$ and $^{15}N$ dimensions are optimized, and seduce1 $^{13}CO$ decoupling eliminates the signal decay due to $^{1}J_{NCO}$ and $^{1}J_{CACO}$, giving rise to intensity enhancement in detected $^{1}H$ resonances. Therefore, this 2D TS CN-H HSQC pulse sequence (Figure 1A) was established as a robust building block for the 3D TS experiments.

The 3D 2TS CN-CN-H HSQC-NOESY-HSQC experiment described demonstrates that it is possible to implement two TS blocks in a 3D pulse scheme. This single 3D experiment produces four 3D spectra and total $^{1}H_C$ and $^{1}H_N$ NOE correlations for a mid-sized protein in a $H_2O$ solution, reflecting a time savings of four times compared to a conventional experiment or two times compared to a 3D TS experiment. These spectra share the improvements made in the 2D TS HSQC experiment (*vide supra*) and are observed to have satisfactory water suppression and comparable sensitivity as the 3D TS H-CN-H NOESY-HSQC spectra. Most importantly, the 3D 2TS data set provides NOE assignments by spin labeling NOE with $^{13}C$ or $^{15}N$ frequencies, greatly improving the chances of unambiguous assignments of many $^{1}H$-$^{1}H$ NOEs, where $^{1}H$ resonances are extensively superimposed. The error of collecting many separate NOESY spectra is reduced, the new experimental methods leading to a greater chance of correct assignment in automatic structure determination protocols: ARIA (Nilges et al., 1997) and SANE (Duggan et al., 2001). Examples of the assignments of two remote NOEs are demonstrated. These NOEs are critical for protein structure determination using interproton distance restraints.

The 3D 2TS CN-CN-H HSQC-NOESY-HSQC experiment described is to be integrated into a suite of multidimensional and multinuclear protein NMR experiments. The enhancement in spectral resolution achieved in this experiment should simplify the process and shorten the time in combined analysis of NMR data to derive molecular geometry restraints. We are encouraged by the results obtained and by taking a step forward towards acceleration of protein structure determination, which is a critical element in achieving better understanding of complex biological systems.

## Acknowledgements

This work is supported by grants from NIH to Xiaolian Gao (GM49957) and by a grant to the Northeast Structural Genomics Consortium from the Protein Structure Initiative of the NIH (P50 GM62413), and the Ontario Research and Development Challenge Fund to Cheryl H. Arrowsmith. We thank Drs Karen L. Maxwell and Glen Legge for useful discussions and helpful comments. The pulse sequences and AU programs are available at http://www.chem.uh.edu/Faculty/Gao/ResearchWebpages/index.html.

## References

Anonymous (1998) *Nat. Struct. Biol.*, **5**, 1019–1020.
Bax, A., Clore, G.M., Driscoll, P.C., Gronenborn, A.M., Ikura, M. and Kay, L.E. (1990) *J. Magn. Reson.*, **87**, 620–627.
Boelens, R., Burgering, M., Fogh, R.H. and Kaptein, R. (1994) *J. Biomol. NMR*, **4**, 201–213.
Brenner, S.E. (2001) *Nat. Rev. Genet.*, **2**, 801–809.
Brutscher, B., Boisbouvier, J., Kupce, E., Tisne, C., Dardel, F., Marion, D. and Simorre, J.P. (2001) *J. Biomol. NMR*, **19**, 141–151.
Cavanagh, J., Fairbrother, W.J., Palmer III, A.G. and Skelton, N.J. (1996) *Protein NMR Spectroscopy: Principles and Practice*, Academic Press, New York, NY.
Clore, G.M. and Gronenborn, A.M. (1991) *Science*, **252**, 1390–1399.
Clore, G.M., Gronenborn, A.M. and Bax, A. (1998) *J. Magn. Reson.*, **133**, 216–221.
Delaglio, F., Grzesiek, S., Vuister, G.W., Zhu, G., Pfeifer, J. and Bax, A. (1995) *J. Biomol. NMR*, **6**, 277–293.
Diercks T., Coles, M. and Kessler, H. (1999) *J. Biomol. NMR*, **15**, 177–180.
Duggan, B.M., Legge, G.B., Dyson, H.J. and Wright, P.E. (2001) *J. Biomol. NMR*, **19**, 321–329.
Emsley, L. and Bodenhausen, G. (1990) *Chem. Phys. Lett.*, **165**, 469–476.
Farmer II, B.T. (1991) *J. Magn. Reson.*, **93**, 635–641.
Farmer II, B.T. and Mueller, L. (1994) *J. Biomol. NMR*, **4**, 673–687.
Jerala, R. and Rule, G.S. (1995) *J. Magn. Reson.*, **B108**, 294–298.
Kay, L.E., Clore, G.M., Bax, A. and Gronenborn, A.M. (1990) *Science*, **249**, 411–414.
Kupce, E. and Freeman, R. (1995) *J. Magn. Reson.*, **A115**, 273–276.

Marion, D., Kay, L.E., Sparks, S.W., Torchia, D.A. and Bax, A. (1989a) *J. Am. Chem. Soc*., **111**, 1515–1517.
Marion, D., Ikura, M., Tschudin, R. and Bax, A. (1989b) *J. Magn. Reson*., **85**, 393–399.
McCoy, M.A. and Mueller, L. (1992a) *J. Am. Chem. Soc*., **114**, 2108–2112.
McCoy, M.A. and Mueller, L. (1992b) *J. Magn. Reson*., **98**, 674–679.
Meissner, A. and Sørensen, O.W. (2000a) *J. Magn. Reson.*, **142**, 195–198.
Meissner, A. and Sørensen, O.W. (2000b) *J. Magn. Reson*., **140**, 499–503.
Muhandiram, D.R., Farrow, N., Xu, G.Y., Smallcombe, S.H. and Kay, L.E. (1993) *J. Magn. Reson.*, **B102**, 317–321.
Nilges, M., Macias, M.J, ODonoghue, S.I. and Oschkinat H. (1997) *J. Mol. Biol.*, **269**, 408–422.
Nocek, J.M., Huang, K. and Hoffman, B.M. (2000) *Proc. Natl. Acad. Sci. USA*, **97**, 2538–2543.
Pascal, S.M., Muhandiram, D.R., Yamazaki, T., Forman-Kay, J.D. and Kay, L.E. (1994) *J. Magn. Reson.*, **103**, 197–201.
Pervushin, K., Braun, D., Fernandez, C. and Wüthrich, K. (2000) *J. Biomol. NMR*, **17**, 195–202.
Pervushin, K.V., Wider, G., Riek, R. and Wüthrich, K. (1999) *Proc. Natl. Acad. Sci. USA*, **96**, 9607–9612.
Šali, A. (1998) *Nat. Struct. Biol.*, **5**, 1029–1032.
Sattler, M., Maurer, M., Schleucher, J. and Griesinger, C. (1995) *J. Biomol. NMR*, **5**, 97–102.
Shaka, A.J., Barker, P.B. and Freeman, R. (1985) *J. Magn. Reson.*, **64**, 547–552.
Tjandra, N. and Bax, A. (1997) *Science*, **278**, 1111–1114.
Tjandra, N., Grzesiek, S. and Bax, A. (1996) *J. Am. Chem. Soc.*, **118**, 6264–6272.
Vis, H., Boelens, R., Mariani, M., Stroop, R., Vorgias, C.E., Wilson, K.S. and Kaptein, R. (1994) *Biochemistry*, **33**, 14858–14870.
Wagner, G. (1989) *Meth. Enzymol.*, **176**, 93.
Xia, Y., Man D. and Zhu, G. (2001) *J. Biomol. NMR*, **19**, 355–360.
Xia, Y., Sze, K. and Zhu, G. (2000) *J. Biomol. NMR*, **18**, 261–268.
Zhang, O. and Forman-Kay, J.D. (1997) *Biochemistry*, **36**, 3959–3970.
Zhu, G., Xia, Y., Sze, K. and Yan, X. (1999) *J. Biomol. NMR*, **14**, 377–381.
Zuiderweg, E.R.P. and Fesik, S.W. (1989) *Biochemistry*, **28**, 2387–2391.